Buckling Analysis and Optimisation of Variable Angle Tow Composite Plates

Zhangming Wu[a], Paul M Weaver[b], Gangadharan Raju[a], Byung Chul Kim[a]

[a]*Research Assistant, Advanced Composite Centre for Innovation and Science, Department of Aerospace Engineering, Queen's Building, UniversityWalk.*
[b]*Professor in Lightweight Structures, Advanced Composite Centre for Innovation and Science, Department of Aerospace Engineering, Queen's Building 2.39, University Walk.*

Abstract

Variable Angle Tow (VAT) placed composite laminates, where the fibre orientations continuously varying over the plane of each ply, generally exhibit variable stiffness properties. The stiffness tailoring of VAT plates through the design of fibre orientation distributions can substantially improve the buckling resistance, which is mainly due to the benign, non-uniform, in-plane load redistribution. In this work, a new mathematical definition is proposed to represent the general variation of fibre-orientation in the VAT plate. In this definition, the coefficients of polynomials are directly equal to the designed fibre angles at pre-selected control points. A Rayleigh-Ritz approach is used to determine the prebuckling loads distributions and critical buckling load of VAT plates. It provides a more efficient means to evaluate the buckling load of VAT laminates, compared with other numerical solutions. Subsequently, preliminary optimisation of VAT plates for maximum buckling load is done using the proposed definition of nonlinear variation of fibre angles. Results obtained for simply supported square VAT plates are compared with optimal results reported in the literature. Finally, long VAT plates with one free edge and others simply supported are studied to demonstrate the viability of the proposed modelling strategy.

Keywords: Variable Angle Tow Plates, Composite, Laminates, Buckling, Optimisation

*Corresponding author
Email address: paul.weaver@bristol.ac.uk (Paul M Weaver)

1. Introduction

Usage of composite structures in aerospace applications has significantly increased in the last decade and the buckling performance is often the primary design criterion of these structures. The buckling resistance of conventional composite laminates with constant ply angles is achieved by the arrangement of ply stacking sequence through the thickness and results in constant stiffness properties across the planform of the plate with tailorability limited to the through-thickness direction. The principle of variable angle tow placement allows fibre orientations to change with position over the entire plane of a ply and results in varying in-plane stiffness properties. This provides the designer more tailoring options to design composite plates with desired stiffness and buckling resistance. Previous work [1, 2, 3, 4, 5, 6] has extensively demonstrated the significant improvement of buckling load carrying capability of variable stiffness composite laminates utilising VAT concepts and these works generally relied on finite element modelling to perform structural analysis of VAT plates. In our work, a novel fibre orientation representation strategy and improved analytical models based on Rayleigh-Ritz method are presented for the buckling analysis of VAT plates.

Different schemes to define the tow-steering fibre paths (orientations) in variable stiffness plates have been presented previously. Nagendra *et al.* [3] employed NURBS (Non-uniform rational B-spline) curves to construct manufacturable fibre paths with a fixed number of control points. Honda *et al.* [7] used a linear combination of B-spline functions to represent the fibre paths varying along one direction. Gürdal and Olmedo [8] proposed the definition of linearly varying fibre orientations, which can be mathematically described by three independent angles ($\phi\langle T_0|T_1\rangle$). The linear variation of fibre angles has been widely adopted in the analysis, design and manufacture [4, 2, 9, 10, 5] of tow-steered composite structures. Later, Parnas *et al.* represented the fibre angles in terms of either Bezier curves or cubic polynomials [11]. Setoodeh *et al.* [12, 13] extended linear variation of fibre orientations into a nonlinear form using Lobatto polynomials and the fibre angles vary along both x, y directions. However, the coefficients of Lobatto polynomials were not directly related to the fibre angles. In this work, an alternative definition of the nonlinear distribution of fibre angles based on Lagrangian polynomials is proposed, in which the coefficients of the polynomials are directly equal to the fibre angles at a set of pre-selected reference points. By independently varying the fibre angles at each reference point and

using sufficient terms of in-plane polynomials, an extended design space for VAT plates can be achieved, compared to linear variations.

For variable stiffness plates subjected to compressive loads, the distribution of in-plane prebuckling stresses is often non-uniform and requires accurate determination in advance of buckling analysis [2]. Solving the prebuckling problem efficiently and accurately is important for the evaluation of buckling load of VAT plates [5]. Olmedo and Gürdal [2] applied the Rayleigh-Ritz method to analyse the buckling response of VAT plates with linearly varying fibre angles. They presented the results of two specific examples, for which the closed-form expressions of prebuckling resultants were available. For the general prebuckling problem, they used a numerical tool (ELLPACK) to solve the coupled in-plane equilibrium equations on displacement fields (u, v) with variable coefficients. This approach requires an iterative procedure to achieve converged displacement solutions and requires relatively significant computational effort. Other recent work on the buckling analysis and design of VAT plates mainly relied on the finite element method (FEM) [14, 6]. The FEM models of VAT plates requires an additional routine to discretize the fibre orientations for each ply and requires more elements to capture the fibre distribution than is usually required to capture an accurate mode shape [6]. The FEM models provide accurate solutions, but require more computational effort when combined with optimisation algorithms to design VAT plates. In this paper, a more efficient and robust model based on the Rayleigh-Ritz method is developed to perform both the prebuckling and buckling analysis of VAT plates subject to axial compressive loads. The model formulation is based on the works proposed by Martin and Leissa [15] and Pandey *et al.* [16], however their approaches were limited to specific boundary conditions and loading cases. The extended new model overcomes these limitations and is suitable for the buckling analysis of compressive loaded VAT plates under general boundary conditions.

Unlike conventional composite laminates, the design of variable stiffness plates is complicated because of the number of variables involved in designing continuous tow steered fibre paths for each ply in the laminate. Ghiasi *et. al.* [17] presented a thorough review of the advantages and limitations of various optimisation techniques used in the design of variable stiffness composite plates. Lund *et. al.* [18] used a discrete material optimisation approach to design laminated hybrid composite plates with variable stiffness for maximum buckling load. They used a gradient based technique and mathematical programming to compute the optimal fibre angle distribution

in the composite laminate. Setoodeh *et. al.*[14] proposed a reciprocal approximation technique to design VAT plates for maximum buckling load and used nodal fibre angles as design variables. In their approach, the computational effort significantly increases with the increase in number of design variables associated with increased mesh density. IJsselmuiden*et. al.* [6] used lamination parameters to design VAT plates for maximum buckling load and this approach was shown to considerably reduce the number of design variables. However, it requires additional effort to convert the optimal lamination parameters distribution results into manufacturable continuous fibre path distribution across the planform of the plate [12, 19]. Tatting *et. al.* used a three parameter curvilinear fibre path definition and a genetic algorithm to design VAT plates for maximum buckling load. The linear fibre angle variation along a particular direction results in a restricted design space and limits the tailorability options. The design space can be expanded by allowing the fibre orientation to vary in both principle directions. The design problem based on the proposed fibre angle representation is non-convex and a Genetic Algorithm (GA) was chosen to solve the optimisation problem. Note, GAs are a well-established global search algorithm based on the theory of evolution [20] and are capable of modelling nonconvex optimum problems. Applications of GA for the buckling design of composite laminates have been done previously [21, 22, 23], for example Le Riche and Haftka used a GA to design laminates stacking sequence [21]. The accuracy, speed and efficiency of the proposed Rayleigh-Ritz model for the buckling analysis of VAT plates reduces the computational effort required by a GA to perform a global research.

In this paper, a new mathematical description based on Lagrange polynomials is presented to define the general distribution of fibre angles varying in the x, y directions. A numerical model based on the Rayleigh-Ritz method is developed for the prebuckling and buckling analysis of VAT plates subject to uniaxial compression. The novel aspect of the Rayleigh-Ritz formulation provides generality to model both the load and displacement boundary conditions for in-plane analysis of VAT plates effectively. The effect of anisotropic flexural-twisting coupling was considered in the buckling analysis of VAT plates for different plate boundary conditions. The buckling loads of VAT plates with linear variation (LV) of fibre angles were first evaluated using the proposed model and the results were validated using FEM. Then, a GA was applied to compute the optimal nonlinear fibre angle distribution of different layups for maximum buckling load under simply supported and free edge

boundary conditions.

2. VAT laminates

The variable stiffness plate concept realized by using advanced tow placement techniques provides considerable freedom for stiffness tailoring in structural design. Understanding of the mechanics behind the improvement of structural performance of VAT laminates is essential for a good design. A mathematical description of either the steered fibre paths or the varying fibre orientations is prerequisite for the study of VAT laminates. In this work, the definition expressed in terms of fibre angles is used for VAT plate design as it is more sensitive to stiffness and strength tailoring criteria. The fibre angle distribution is then used to generate manufacturable curvilinear tow paths for the VAT laminates. In this work, a polynomial description was chosen to represent the fibre angle definition because of its generality and is explained in the following subsections.

2.1. Linear variation of fibre orientation

The linear variation of fibre orientation angles is defined by [5],

$$\theta(x') = \phi + T_0 + (T_1 - T_0)\frac{|x'|}{d} \tag{1}$$

where T_0 and T_1 are fibre angles at two prescribed reference points (A and B) respectively, d is the distance between points (A, B) and ϕ is the angle of rotation of the fibre path[5].

2.2. Nonlinear variation of fibre orientation

In general, nonlinear distributions of fibre orientations on an $x - y$ plane can be represented by a double series function, for example the Lobatto polynomials[13]. In order to give a clearer description for fibre angles, the nonlinear variation (NLV) of fibre orientations is now defined and is based on a set of $M \times N$ pre-selected reference points in the plate domain, as illustrated in Fig. 1. A double series function of $(M-1)^{th}$ by $(N-1)^{th}$ order polynomials is used to fit the nonlinear distribution of fibre angles. The coefficients of polynomials are determined by the fibre angles at those reference points and by using any orthogonal polynomial series the fibre angle distribution can be uniquely determined for the chosen fibre angle at each reference point. In

this paper, Lagrangian polynomials are used and the nonlinear variation of fibre orientation angles is expressed in the following form,

$$\theta(x,y) = \sum_{m=0}^{M-1}\sum_{n=0}^{N-1} T_{mn} \cdot \prod_{m\neq i}\left(\frac{x-x_i}{x_m-x_i}\right) \cdot \prod_{n\neq j}\left(\frac{y-y_j}{y_n-y_j}\right) \tag{2}$$

where $(x_i, y_j), (x_m, y_n)$ are the $x-y$ coordinates of reference points. The advantage of using the Lagrangian polynomials in Eq. (2) to represent the nonlinear distribution of fibre angles is that the coefficient of each term (T_{mn}) is also the fibre angle at a specific reference point (x_m, y_n). If the fibre angle is only allowed to vary along an axis, for example the x axis, Eq. (2) simplifies to

$$\theta(x) = \sum_{m=0}^{M-1} T_m \cdot \prod_{m\neq i}\left(\frac{x-x_i}{x_m-x_i}\right) \tag{3}$$

Similarly, for the given angle of rotation of fibre path ϕ, Eq. (3) changes to

$$\begin{cases} \theta(x,y) = \phi + \theta(x') = \phi + \sum_{m=0}^{M-1} T_m \cdot \prod_{m\neq i}\left(\frac{x'-x'_i}{x'_m-x'_i}\right) \\ x' = x\cos(\phi) + y\sin(\phi) \end{cases} \tag{4}$$

When only two reference points ($M = 2$ and $x_0 = 0, x_1 = d$) are used, Eq. (3) simply reduces to the same definition of linear variation of Eq. (1).

Generally, the grid reference points can be chosen randomly and not necessarily to be uniform. However, a good selection of reference points will accelerate the optimisation process and avoid entrapment in local minima. The choice of number and positions of reference points largely depends on specific VAT plate geometry, boundary conditions and loading cases.

3. Theoretical Modelling

3.1. Prebuckling

For a plate subject to given boundary forces (N_0), the plane elasticity problem is solved by minimising the total potential energy (Π_p), expressed in terms of displacement fields (u, v) as[15],

$$\Pi_p = \Pi_s(u,v) - \int_{C_1} (N_{x\nu 0}u + N_{y\nu 0}v)ds \tag{5}$$

where Π_s is the elastic strain energy of the plate. This approach was found to be intractable in determining the prebuckling analysis of VAT plate loaded by prescribed displacements. The main reasons are that the distribution of boundary forces corresponding to displacement boundary conditions is unknown and implicit, and also, minimisation of the potential energy fails to identify the coupled relation between the displacement fields (u, v) and unknown edge forces. Nevertheless, the study on prescribed displacement boundary conditions is important for either structural testing or practical loading cases. Closed-form solution for some specific cases of VAT plates loaded under uniform edge compression were given by Gürdal and Olmedo [8, 2]. In the current work, a generalised approach based on Castigliano's principle is applied to solve the prebuckling problem of VAT plates. In this approach, the in-plane equilibrium equations of the VAT plate are expressed using Airy's stress function. The condition of compatibility and prescribed displacement boundary conditions are satisfied through minimisation of the total complementary energy, given by [24],

$$\Pi_c = \Pi_s - \int_{C_2} (u_0 N_{x\nu} + v_0 N_{y\nu}) ds \tag{6}$$

The stress resultant distributions $\mathbf{N}$ are derived from the Airy stress function as follows [25],

$$N_x = \frac{\partial^2 \Phi}{\partial y^2}, \quad N_y = \frac{\partial^2 \Phi}{\partial x^2}, \quad N_{xy} = -\frac{\partial^2 \Phi}{\partial x \partial y} \tag{7}$$

The mid-plane strains are also rewritten in terms of Φ as,

$$\begin{aligned} \epsilon_x^0 &= a_{11}\frac{\partial^2 \Phi}{\partial y^2} + a_{12}\frac{\partial^2 \Phi}{\partial x^2} - a_{16}\frac{\partial^2 \Phi}{\partial x \partial y} \\ \epsilon_y^0 &= a_{12}\frac{\partial^2 \Phi}{\partial y^2} + a_{22}\frac{\partial^2 \Phi}{\partial x^2} - a_{26}\frac{\partial^2 \Phi}{\partial x \partial y} \\ \gamma_{xy}^0 &= a_{16}\frac{\partial^2 \Phi}{\partial y^2} + a_{26}\frac{\partial^2 \Phi}{\partial x^2} - a_{66}\frac{\partial^2 \Phi}{\partial x \partial y} \end{aligned} \tag{8}$$

where $a_{ij}(i, j = 1, 2, 6)$ are the inverse of the in-plane stiffness matrix (A). Combined with Eqs. (7) and (8), the complementary energy Π_c of Eq. (6)

can be expressed purely by a single function Φ. The following form of complementary energy with respect to normalised coordinates $\xi = 2x/a$, $\eta = 2y/b$ ($\xi, \eta \in [-1, 1]$) is derived for the convenience of analysis,

$$\begin{aligned}\Pi_c =& \frac{2b}{a^3}\int_{-1}^{1}\int_{-1}^{1}\left[\mu^4 a_{11}(\xi,\eta)\left(\frac{\partial^2\Phi}{\partial\eta^2}\right)^2 + a_{22}(\xi,\eta)\left(\frac{\partial^2\Phi}{\partial\xi^2}\right)^2 + \right.\\ & 2\mu^2 a_{12}(\xi,\eta)\frac{\partial^2\Phi}{\partial\xi^2}\frac{\partial^2\Phi}{\partial\eta^2} + + a_{66}(\xi,\eta)\left(\frac{\partial^2\Phi}{\partial\xi\partial\eta}\right)^2\\ & \left. - 2\mu^3 a_{16}(\xi,\eta)\frac{\partial^2\Phi}{\partial\eta^2}\frac{\partial^2\Phi}{\partial\xi\partial\eta} - 2\mu a_{26}(\xi,\eta)\frac{\partial^2\Phi}{\partial\xi^2}\frac{\partial^2\Phi}{\partial\xi\partial\eta}\right]d\xi d\eta\\ & - \frac{2}{a}\left(\mu\int_{-1}^{1}\left[\frac{\partial^2\Phi}{\partial\eta^2}u - \frac{\partial^2\Phi}{\partial\xi\partial\eta}v\right]_{\xi=1}d\eta + \int_{-1}^{1}\left[\frac{\partial^2\Phi}{\partial\eta^2}u - \frac{\partial^2\Phi}{\partial\xi\partial\eta}v\right]_{\xi=-1}d\eta\right)\\ & - \frac{2}{a}\left(\int_{-1}^{1}\left[\frac{\partial^2\Phi}{\partial\xi^2}v - \frac{\partial^2\Phi}{\partial\xi\partial\eta}u\right]_{\eta=1}d\xi + \mu\int_{-1}^{1}\left[\frac{\partial^2\Phi}{\partial\xi^2}v - \frac{\partial^2\Phi}{\partial\xi\partial\eta}u\right]_{\eta=-1}d\xi\right)\end{aligned} \tag{9}$$

where μ is the plate aspect ratio (a/b). The force function Φ is expressed in a separate form [16, 26, 27] as,

$$\Phi(\xi,\eta) = \Phi_0(\xi,\eta) + \Phi_1(\xi,\eta) \tag{10}$$

where $\Phi_0(\xi,\eta)$ satisfies the applied force distribution along the edges of the VAT plate, which is an unknown function in the case of prescribed displacement boundary conditions. The second term $\Phi_1(\xi,\eta)$ in Eq. (10) satisfies the stress free boundaries and is expanded into a series form [16, 26, 27],

$$\Phi_1(\xi,\eta) = \sum_{p=0}^{P}\sum_{q=0}^{Q}\phi_{pq}X_p(\xi)Y_q(\eta) \tag{11}$$

It is observed that the stress-free constraints for Φ_1 are analogous to geometric boundary conditions of the clamped edges and the corresponding admissible functions are applied to $X_p(\xi)$ and $Y_q(\eta)$ [16].

The general prebuckling problem is solved by minimising the complementary energy of Eq. (9). However, the expression for $\Phi_0(\xi,\eta)$, as well as the model implementation, varies with the in-plane boundary conditions and loading cases [28]. In the current work, the following assumptions were

considered for the in-plane analysis of VAT plates: (a) the plate is symmetric and balanced about its midplane, thus no extension-shear coupling exists ($A_{16} = 0, A_{26} = 0$); (b) the plate is subject to an uniform displacement compressive loading ($x = \pm\frac{a}{2}$:$u = \mp\frac{\Delta_x}{2}$), and the transverse edges are allowed to deform freely, therefore the edges are stress-free ($N_{y0} = 0, \quad N_{xy0} = 0$) (Fig. 2).

The function Φ_0 is only related to the unknown lateral boundary forces (N_{x0}) and is expanded into the following series,

$$N_{x0} = \frac{4}{b^4}\frac{\partial^2 \Phi_0(\eta)}{\partial \eta^2} = \frac{4}{b^4}\sum_{k=0,1,2,\cdots}^{K} c_k \psi_k(\eta), \tag{12}$$

where c_k are the undetermined coefficients for the force distribution along the edge and ψ_k is an admissible function. When only one term is used in the above series, it represents the case of uniform compression loading.

Substituting Eqs. (10,11,12) into Eq. (9) and minimising the total complementary energy Π_c^* with respect to the unknown coefficient ϕ_{pq}, c_k, a set of linear algebraic equations is obtained and expressed in the following matrix form:

$$\begin{bmatrix} \mathbf{U} & \mathbf{Uc} \\ \mathbf{Uc}^T & \mathbf{C} \end{bmatrix} \begin{bmatrix} \phi \\ c \end{bmatrix} = \begin{bmatrix} \mathbf{O} \\ \mathbf{P_{x0}} \end{bmatrix} \tag{13}$$

where the matrices $\mathbf{U}$ and $\mathbf{C}$ are the components of strain energy (Π_s) expanded by the series of Φ_1 and Φ_0, respectively. The matrix $\mathbf{Uc}$ denotes the coupling between the function Φ_1 and Φ_0 in the strain energy, $\mathbf{O}$ is a null matrix and $\mathbf{P_{x0}}$ is the part of the boundary integral expanded by the function Φ_0. The detailed expressions of the elements in the matrices are presented in the Appendix. Eq. (13), is solved for the unknown coefficients ϕ_{pq}, c_k and are used to compute the in-plane stress distribution of VAT plates using the equations (7) and (10).

3.2. Buckling

The Rayleigh-Ritz method is then applied to solve the buckling problem of VAT plates by using the stress distribution results from in-plane analysis of VAT plates. The potential energy (Π_b) of a VAT plate under bending is expressed using the transverse displacement (w) and the force function (Φ) in the following form,

$$
\begin{aligned}
\Pi_b =& \frac{2b}{a^3}\int_{-1}^{1}\int_{-1}^{1}\Bigg[D_{11}(\xi,\eta)\left(\frac{\partial^2 w}{\partial \xi^2}\right)^2+\mu^4 D_{22}(\xi,\eta)\left(\frac{\partial^2 w}{\partial \eta^2}\right)^2+\\
&2\mu^2 D_{12}(\xi,\eta)\frac{\partial^2 w}{\partial \xi^2}\frac{\partial^2 w}{\partial \eta^2}+4\mu^2 D_{66}(\xi,\eta)\left(\frac{\partial^2 w}{\partial \xi \partial \eta}\right)^2+\\
&4\mu D_{16}(\xi,\eta)\frac{\partial^2 w}{\partial \xi^2}\frac{\partial^2 w}{\partial \xi \partial \eta}+4\mu^3 D_{26}(\xi,\eta)\frac{\partial^2 w}{\partial \eta^2}\frac{\partial^2 w}{\partial \xi \partial \eta}\Bigg]d\xi d\eta\\
&+\frac{2}{ab}\lambda\int_{-1}^{1}\int_{-1}^{1}\left[\frac{\partial^2 \Phi}{\partial \eta^2}\left(\frac{\partial w}{\partial \xi}\right)^2+\frac{\partial^2 \Phi}{\partial \xi^2}\left(\frac{\partial w}{\partial \eta}\right)^2-\frac{\partial^2 \Phi}{\partial \xi \eta}\frac{\partial w}{\partial \xi}\frac{\partial w}{\partial \eta}\right]d\xi d\eta
\end{aligned}
\tag{14}
$$

The transverse displacement (w) is expanded into a series and is required to satisfy the plate boundary conditions [29],

$$
w(\xi,\eta)=\sum_{m=0}^{M}\sum_{n=0}^{N}A_{mn}X_m(\xi)Y_n(\eta) \tag{15}
$$

Substituting Eq. (15) and prebuckling solutions of Eq. (13) into $\Pi_b(\xi,\eta)$ and minimising the potential energy with respect to A_{mn}, the critical buckling load is given by the lowest eigenvalue of the following matrix,

$$
\{\mathbf{K}+\lambda\mathbf{L}\}\{\mathbf{A}\}=0 \tag{16}
$$

where [**K**] is the bending stiffness matrix of VAT plate and [**L**] is the stability matrix of VAT plate due to the in-plane stress fields. The expressions for the matrices [**K**] and [**L**] are presented in the Appendix. The vector $\mathbf{A}=[A_{00},A_{01},A_{10},\cdots,A_{MN}]$ contains the elements of out-of-plane displacement and defines the corresponding buckling mode shape.

After the eigenvalue (λ_{cr}) of Eq. (16) is obtained, the average edge compression loading per unit length ($\hat{N}_x^{cr}$) is used to represent the critical buckling load,

$$
\hat{N}_x^{cr}=\frac{\lambda_{cr}}{b}\int_{-\frac{b}{2}}^{\frac{b}{2}}\frac{\partial^2 \Phi_0}{\partial y^2}dy \tag{17}
$$

Two different forms of the normalized buckling coefficients are used for the VAT plates in this paper, as following,

$$
K_x^{cr}=\frac{\hat{N}_x^{cr}a^2}{E_1 h^3},\quad K_x^{*}=\frac{(\hat{N}_x^{cr})_{vat}}{(N_x^{cr})_{iso}} \tag{18}
$$

The first one is expressed with respect to the longitudinal Young's modulus (E_1) for the specific purpose of comparison with literature results [5, 6]. An alternative form (K_x^*) is defined by the ratio of its average buckling load to that of a corresponding homogeneous quasi-isotropic laminate. The latter gives a direct measure of performance over a realistic laminate. The evaluation of buckling load of a quasi-isotropic laminate based on an equivalent bending stiffness is given by,

$$D_{iso} = \frac{E_{iso}h^3}{12(1-\nu_{iso}^2)}, \quad \nu_{iso} = \frac{U_4}{U_1}, \quad E_{iso} = U_1(1-\nu_{iso}^2) \tag{19}$$

where ν_{iso} and E_{iso} are equivalent Poisson's ratio and equivalent Young's modulus, respectively. U_1, U_2, U_4 are material invariants [30].

3.3. Legendre polynomials

Principally, the admissible functions for the model implementation are chosen to be any complete series, such as trigonometric Fourier series, beam functions or polynomials. The Legendre polynomials are adopted in this work, for the series expansion of the admissible functions, which are $X_p(\xi)$, $Y_q(\eta)$, $\psi_k(\eta)$, $X_m(\xi)$ and $Y_n(\eta)$ in Eqs. (11,12,15). Legendre polynomials capture localised behaviour well due to the non-periodic nature of successive polynomials whilst, on the other hand, trigonometric functions, due to their periodicity, require high frequency modes to capture localised effects [31]. As such, Legendre polynomials tend to yield better convergence properties for localised responses than trigonometric Fourier series. Legendre polynomials are defined as,

$$\begin{aligned} &L_0 = 1,\ L_1 = x,\ L_2 = \frac{1}{2}(3x^2-1)\ \cdots \\ &L_i(x) = \sum_{j=0}^{J}(-1)^j \frac{(2i-2j)!}{2^i j!(i-j)!(i-2j)!}x^{i-2j}. \\ &J = \frac{i}{2}(i=0,2,4,\cdots),\ \ \frac{i-1}{2}(i=1,3,5,\cdots) \end{aligned} \tag{20}$$

To satisfy the stress-free constraints, the admissible functions $X_p(\xi), Y_q(\eta)$ in function $\Phi_1(\xi,\eta)$ are expanded using Legendre polynomials and are given as [16, 26, 27],

$$\begin{aligned} X_p(\xi) &= (1-\xi^2)^2 L_p(\xi) \\ Y_q(\eta) &= (1-\eta^2)^2 L_q(\eta) \end{aligned} \tag{21}$$

Also, the admissible functions $X_m(\xi), Y_n(\eta)$ are expressed using Legendre polynomials to satisfy the geometric boundary conditions of the out-of-plane displacement (w) and is given by,

$$\begin{aligned} X_m(\xi) &= (1-\xi)^\iota (1+\xi)^\iota L_p(\xi) \\ Y_n(\xi) &= (1-\xi)^\iota (1+\xi)^\iota L_q(\eta) \end{aligned} \tag{22}$$

where $\iota = 0, 1, 2$ for free, simply-supported and clamped edges boundary conditions, respectively. Legendre polynomials (or other orthogonal polynomials) also exhibit good convergence properties in the presence of flexural anisotropy (D_{16}, D_{26}) in VAT plates [28].

The efficiency of evaluating the integrations in the matrices of Eqs. (13) and (16) is highly important for the implementation of the Rayleigh-Ritz method. Numerical integration methods can be directly applied, for example the quasi-Monte Carlo method [32]. Alternatively, each function in the stiffness matrices can be expanded into a double Fourier-Legendre series [33] as follows [34],

$$a_{ij}(\xi,\eta) = \sum_{r=0}^{R}\sum_{s=0}^{S} \Gamma_{rs}^{a_{ij}} L_r(\xi) L_s(\eta) \tag{23}$$

$$D_{ij}(\xi,\eta) = \sum_{r=0}^{R}\sum_{s=0}^{S} \Gamma_{rs}^{D_{ij}} L_r(\xi) L_s(\eta) \tag{24}$$

where $i, j = 1, 2, 6$ and the coefficients $\Gamma_{rs}^{a_{ij}}$ are

$$\Gamma_{rs}^{a_{ij}} = \left(\frac{2r+1}{2}\right)\left(\frac{2s+1}{2}\right)\int_{-1}^{1}\int_{-1}^{1} a_{ij}(\xi,\eta) L_r(\xi) L_s(\eta) d\xi d\eta \tag{25}$$

Substituting Eqs. (23,24) into Eqs. (26,14), each integrand is simplified into a sum of several triple products of Legendre polynomials [35], therefore the closed-form solutions of integration can be obtained. The coefficients ($\Gamma_{mn}^{a_{ij}}, \Gamma_{mn}^{D_{ij}}$) may be evaluated numerically in terms of lamination parameters which reduces computational effort. The number of terms (R, S) chosen in the series expansion of Eq. (23,24) depends on the nonlinearity of fibre angles. For linear variation (LV) or any general NLV fibre representation, a significant finding is that only five to seven terms of series expansion along each direction appears to be a good compromise between accuracy and computational effort.

4. Buckling Optimisation

In this paper, a GA [21] is used to determine the optimal distribution of fibre angles for the maximum buckling load of VAT $[\pm\theta_1/\pm\theta_2]_s$ laminates subject to uniform displacement compression. The optimisation procedure is based on the proposed formula of the NLV of fibre-orientation angles (Eq. 2) to design VAT plates for maximum buckling load. The fibre angles at a set of pre-selected reference points are chosen as design variables. In the GA optimal search, a sufficiently large population and generation are used to avoid local optimisation results. Several trials of the GA search with different initial populations were performed to obtain converged results. The crossover and mutation probabilities are chosen to be 0.7 and 0.04. Due to the symmetry of the buckling problem in terms of boundary conditions, geometry and loadings, the fibre angle distribution is designed to be doubly symmetric, that is $\theta(x, y) = \theta(|x|, |y|)$. The reference points, as shown in Figure 1, are chosen to uniformly fill the plate domain to define the NLV of fibre orientations. The optimisation problem is stated as,

Maximize: K_x^{cr}
Design Variables: $[T_{00} \dots T_{mn} \dots T_{M_1N_1}]_{\theta_1}/[T_{00} \dots T_{mn} \dots T_{M_2N_2}]_{\theta_2}$
Subject to: $-\pi/2 \leq T_{mn} \leq \pi/2$

This optimisation problem on the general symmetric laminates that are independent of the number of layers had been studied by IJsselmuiden *et al.* [6] using lamination parameters and a gradient-based optimiser. As the lamination parameters forms a complete design space for general laminates, their results are considered as the upper bound to this problem [36]. The optimisation results for the VAT plates under different plate boundary conditions are presented in the next section.

5. Results and Discussion

5.1. Model Validation

In this section, the convergence of prebuckling and buckling analysis of VAT plates using the Rayleigh-Ritz method is studied and the results are validated using FEM simulation. For all numerical examples, lamina properties are $E_1 = 181$GPa, $E_2 = 10.273$GPa, $G_{12} = 7.1705$GPa, $\nu = 0.28$, with thickness of each equal to $0.127mm$. Square VAT plates ($a = b = 0.254m$) with linear fibre orientation distribution ($[\phi \pm \langle T_0|T_1\rangle]_{2s}$) subject to uniform displacement compression with the transverse edges free to deform and all

the plate edges simply-supported are considered for the model validation. The FEM modelling for the prebuckling and buckling analysis of VAT plates was done using ABAQUS and an additional routine was developed to generate ABAQUS composite elements with independent fibre orientations. The S4 shell element was chosen for discretization of the VAT plate structure and a mesh density of 40×40 was selected to achieve the required accuracy.

A square VAT plate $[0 \pm \langle 45|0\rangle]_{2s}$ is used for the prebuckling model validation. The in-plane stress resultants of the VAT plate under uniform end shortening are nonuniform and vary with the x, y directions [8]. Numerical results of the stress resultant distributions of the VAT plate computed using the Rayleigh-Ritz method and FEM simulation are shown in Fig. 3. The three set of curves in Fig. 3 show the nonuniform variation of the normalised stress resultants across different sections, N_x at $x = a/2$, N_x at $y = b/2$ and N_y at $y = 0$ and the Rayleigh-Ritz results matches well with FEM solution. Fig. 3 also provides information about the number of terms $(P + 1, Q + 1, K + 1)$ required for each series expansion of Φ to achieve accurate stress resultant results.

The numerical convergence of critical buckling load of VAT plates with respect to the number of polynomial terms used in the Rayleigh-Ritz method is examined for two different VAT plate configurations, (a)$[90 \pm \langle 0|75\rangle]_{2s}$; (b)$[0 \pm \langle 45|0\rangle]_{2s}$. The results of buckling coefficient K_x^{cr} of VAT plates with different number of polynomial terms are shown in Fig. 4. It clearly shows the rapid convergence of the results to the FEM solution with the increase in number of polynomial terms. The curves in Fig. 4 correspond to the in-plane stress resultants used for buckling analysis which are determined using different number of terms for the series expansion of Φ in the prebuckling analysis. Fig. 4 indicates that the accuracy of prebuckling solutions have only a slight influence on the evaluation of buckling load and this is because the buckling analysis of VAT plates only takes into account an average effect of in-plane stress fields.

5.2. SSSS Square Laminates

A square, symmetric and balanced VAT laminate ($[\pm\theta_1/\pm\theta_2]_s$) subject to axial compression and simply supported boundary condition is considered in this study. A GA was applied to determine the optimal fibre representations for maximum buckling load and the results are shown in Table 1. The buckling load results of the first two modes closely match and are listed in Table 1. To achieve good accuracy, 7 terms of Legendre polynomials were

used for prebuckling analysis and 9 terms were used for buckling analysis. The FEM results are shown in parentheses in Table 1 for the validation. In each optimal design, different configurations of reference points (design variables) for the NLV fibre angles were used and are illustrated in Fig. 5. The corresponding fibre angles at reference points of each design are given in Table 2. Using Eq. (2), the distributions of fibre angles in the VAT plate can be explicitly determined. If the fibre angles are varying along one direction, the fibre tow trajectories can be directly determined via the numerical integration of $tan(\theta)$ [7]. The streamline approach was used for determining the smooth tow trajectories in the plate for the fibre angles varying with both axes directions (NLV(x, y)) [12].

The optimal results in Table 1 for maximum buckling load closely matches the results given in IJsselmuiden *et al.*'s work [6]. Although the transverse edges in [6] are defined to remain straight, it was found that the difference in the results from our freely deforming (stress free) condition was small. The first VAT plate (#1) optimal design is based on fibre variation only in the transverse direction and the buckling load result matches well. As shown in Table 2, only 3 reference points were used to design each layup and results in a parabolic distribution of fibre angles. The remaining two VAT plate designs are based on nonlinear fibre variation in both the directions $\theta = \theta(x, y)$. For the second VAT plate, 3-by-3 design variables ($M_1, M_2 = 3, N_1, N_2 = 3$) are used for each layer as shown in Fig. 5. The third VAT plate (#3) is obtained from the second result but the inner layers ($[\pm\theta_2]_s$) are re-designed by using more reference points (5-by-5), resulting in further improvement of buckling load. The fibre angle distributions and the buckling load results matches well with results presented by van Campen and Gürdal [19]. Note, the flexural-twisting coupling (D_{16}, D_{26}) for the symmetric laminates are considered in the computation of critical buckling load in this work, whereas it is ignored in [6] and [19].

Figs. 6 and 7 illustrate the nonuniform stress resultant distribution and the first two buckling modes shapes of an optimal VAT plate (#2), respectively. The results obtained using the Rayleigh-Ritz method matches well with FEM and thus it clearly shows the robustness of the proposed models. Fig. 6 shows that the stress resultant (N_x) redistribute away from the central region of the plate towards the transverse edges and confirms that load redistribution is the main driver for buckling improvement of VAT plates [2, 5, 6]. The buckling modes of the optimal VAT plate shown in Fig. 7 are analogous to the buckling patterns of orthotropic plates and this behaviour indicates the

Table 1: Optimal results for maximum buckling load (K_x^{cr}) of 8-layer square laminates $[\pm\theta_1/\pm\theta_2]_s$ by using NLV fibre orientations. FEM results are shown in parentheses for comparison.

Design No.	NLV Optimal results		LP Optimal results [6]		Difference
	1^{st} Mode	2^{nd} Mode	1^{st} Mode	2^{nd} Mode	
#1:NLV(y)	3.4991 (3.4990)	3.5026 (3.5058)	3.5355	3.8054	1%
#2:NLV(x, y)	3.7112 (3.6750)	3.7227 (3.6973)	3.9989	4.0473	7.2%(8.1%)
#3:NLV(x, y)	3.7849 (3.7341)	3.8054 (3.7607)	3.9989	4.0473	5.3%(6.6%)

Table 2: The fibre angles for each optimal design of VAT plate

Design No.	Fibre Angles at Reference Points	
	$+\theta_1$	$+\theta_2$
#1	$T_{0,1,2} = [68, 55, 19]$	$T_{0,1,2} = [-76, -55, 9]$
#2	$T_{mn} = \begin{bmatrix} 71 & 49.5 & 71.5 \\ 67 & 50 & 51 \\ 17 & 12 & 45 \end{bmatrix}$	$T_{mn} = \begin{bmatrix} -72.5 & -59 & -59.5 \\ -65 & -54 & -50.5 \\ 14 & 11.5 & 6 \end{bmatrix}$
#3	$\theta_1 : \#2$	$T_{mn} = -\begin{bmatrix} 89 & 67.5 & 64 & 65 & 82 \\ 81 & 69 & 65 & 60 & 60 \\ 80.5 & 66.5 & 58 & 54.5 & 59 \\ 26 & 25 & 18 & 24 & 25 \\ 8 & -4.5 & 1 & -5 & -0 \end{bmatrix}$

effects of flexural anisotropy (D_{16}, D_{26}) of laminates was suppressed for the optimal design of maximum buckling performance. The suppression of flexural anisotropy was achieved through designing the fibre angles distribution of $+\theta_1$ and $+\theta_2$ to be opposite directions, as illustrated in Table 2.

5.3. SSSF Long Laminates

In this section, the buckling analysis of long VAT plates with one edge free and others simply supported is studied using the Rayleigh-Ritz method. The length of the VAT plate was selected to be 20 times its width ($\mu = 20$) to model a long structure, such as a stringer (or half flange of an I-section), in which the boundary conditions at the short ends have little influence on buckling performance. From the discussions above, it is clear that the lateral load redistribution is the main contribution to buckling improvement of VAT plates subjected to uniaxial compression. Thus, only the cases of transversely varying fibre orientations, $\theta = \theta(y)$, are chosen for the preliminary study of this problem. The buckling mode shape of the long plate did not possess any symmetry along the y direction and thus, two reference points for LV

Table 3: Optimal results for maximum buckling load of long SSSF 8-layer laminates

Lay-ups	Fibre Angles at Ref-points	Buckling load (N)	K_x^*	Increase
Quasi-Iso	—	112.61	1	-
$[\pm 45]_{2s}$	—	168.47 (168.32)	1.50	-
LV(y),$[\pm\theta]_{2s}$	$T_{0,1} = [80, 10]$	309.78 (309.53)	2.76	176%
NLV(y),$[\pm\theta]_{2s}$	$T_{0..2} = [52, -7, 59]$	337.79 (334.3)	3.01	201%
LV(y),$[\pm\theta_1/\pm\theta_2]_s$	$+\theta_1 : T_{0,1} = [72, 24]$ $+\theta_2 : T_{0,1} = [-80, 5.5]$	371.72 (370.75)	3.31	231%
NLV(y),$[\pm\theta_1/\pm\theta_2]_s$	$+\theta_1 : T_{0..2} = [51, 12, 62.5]$ $+\theta_2 : T_{0..2} = [-50, 14, -66]$	397.74 (395.56)	3.55	255%

fibre representation are chosen at $y = 0$ (T_0) and $y = b$ (T_1). For the parabolic distribution of fibre angle, three reference points located at $y = 0, b/2, b$ (T_0, T_1, T_2) were used. Fig. 8 illustrates a segment of tow trajectories formed by parabolically varying fibre angles in a long SSSF laminate.

Optimal buckling coefficient results of VAT plates with either LV or NLV fibre angles obtained using our standard GA search are listed in Table 3. A mesh density of 200×10 was chosen for the FEM analysis and the results are presented in Table 3 within parentheses for validation. The results show significant increase of buckling load up to 255% can be achieved for the SSSF long VAT laminates with an 8-layer balanced symmetric lay-up. This improvement is due to the redistribution of the compression load away from the free edge towards the simply supported edge. It is observed that parabolically varying the fibre angles has nearly a 20% gain in the buckling load compared to LV fibre angles. The buckling mode shape of the VAT plate with NLV(y) of fibre representation ($[\pm\theta_1/\pm\theta_2]_s$) is computed using the Rayleigh-Ritz method and FEM and is shown in Fig. 9. It is also interesting to note that the buckling mode shape of VAT plates is skewed to one side of the plate, which is not observed for a straight fibre laminate with balanced symmetric lay-ups, but is shown in highly flexural anisotropic laminates [37]. The work of this section also exhibits the robustness of proposed models for the VAT plates involved flexural anisotropy and free edges.

6. Conclusion

In this paper, methodologies based on the Rayleigh-Ritz method were applied for the prebuckling and buckling analysis of general variable stiffness plates. The approaches are applicable to mixed boundary conditions and

were found to be computationally less expensive compared to FEM. Principally, the merits of the new models for VAT plates benefits from utilizing the complementary energy expressed by Airy's stress function and the Legendre polynomials. Numerical results on VAT plates of linearly varying fibre angles demonstrated the accuracy and fast convergence features of those approaches.

A new formula for the nonlinear distribution of fibre angles was proposed, in which the coefficients of polynomials directly reflect the fibre angles at selected reference points. Preliminary optimisation for maximum buckling load of VAT laminates was implemented using a GA and the results obtained were close to published results achieved by using lamination parameters. Consequently, the advantages of using this new representation to describe the fibre angles were demonstrated. The study of an infinitely long VAT plate with one free edge further highlighted the proposed methodologies, as well as the distinct superiority of using variable angle tows for enhanced buckling response of composite laminates.

Acknowledgments

The authors wish to acknowledge EPSRC, Airbus and GKN for supporting this research under the project ABBSTRACT2 (EP/H025898/1).

Appendix

The elements of the matricies in Eq. (13) are expressed as following,

$$
\begin{aligned}
U(\bar{p}\bar{q},pq) = \int_{-1}^{1}\int_{-1}^{1}\Big[&\mu^4 a_{11} X_p Y_{q,\eta\eta} X_{\bar{p}} Y_{\bar{q},\eta\eta} + \\
&\mu^2 a_{12}(X_p Y_{q,\eta\eta} X_{\bar{p},\xi\xi} Y_{\bar{q}} + X_{p,\xi\xi} Y_q X_{\bar{p}} Y_{\bar{q},\eta\eta}) + \\
&a_{22} X_{p,\xi\xi} Y_q X_{\bar{p},\xi\xi} Y_{\bar{q}} + \mu^2 a_{66} X_{p,\xi} Y_{q,\eta} X_{\bar{p},\xi} Y_{\bar{q},\eta} - \\
&\mu^3 a_{16}(X_{p,\xi} Y_{q,\eta} X_{\bar{p}} Y_{\bar{q},\eta\eta} + X_p Y_{q,\eta\eta} X_{\bar{p},\xi} Y_{\bar{q},\eta}) - \\
&\mu a_{26}(X_{p,\xi\xi} Y_q X_{\bar{p},\xi} Y_{\bar{q},\eta} + X_{p,\xi} Y_{q,\eta} X_{\bar{p},\xi\xi} Y_{\bar{q}})\Big] d\xi d\eta \\
Uc(\bar{p}\bar{q},k) = \int_{-1}^{1}\int_{-1}^{1}\Big(&\mu^4 a_{11}\psi_k X_{\bar{p}} Y_{\bar{q},\eta\eta} + \mu^2 a_{12}\psi_k X_{\bar{p},\xi\xi} Y_{\bar{q}} - \\
&\mu^3 a_{16}\psi_k X_{\bar{p},\xi} Y_{\bar{q},\eta}\Big) d\xi d\eta \\
C(\bar{k},k) = \int_{-1}^{1}\int_{-1}^{1} &\mu^4 a_{11}\psi_{\bar{k}}\psi_k d\xi d\eta, \\
P_{x0}(k) = \int_{-1}^{1} &\frac{a}{4}\mu^2\psi_k \Delta_x d\eta;
\end{aligned}
\tag{26}
$$

where $p,\bar{p} = 0,1,2,\cdots,P;\quad q,\bar{q} = 0,1,2,\cdots,Q;\quad k,\bar{k} = 0,1,2,\cdots,K$ and $\bar{p}\bar{q} = \bar{p}(Q+1)+\bar{q};\ pq = p(Q+1)+q.$

The expressions of the matrix $\mathbf{K}$ and $\mathbf{L}$ in Eq. (16) are given by,

$$
\begin{aligned}
K(rs,mn) = & \int_{-1}^{1}\int_{-1}^{1}\Big[D_{11}X_{m,\xi\xi}Y_nX_{r,\xi\xi}Y_s \\
& + \mu^2 D_{12}(X_mY_{n,\eta\eta}X_{r,\xi\xi}Y_s + X_{m,\xi\xi}Y_nX_rY_{s,\eta\eta}) \\
& + \mu^4 D_{22}X_{m,\xi\xi}Y_nX_{r,\xi\xi}Y_s + \mu^2 D_{66}X_{m,\xi}Y_{n,\eta}X_{r,\xi}Y_{s,\eta} \\
& + \mu D_{16}(X_{m,\xi}Y_{n,\eta}X_rY_{s,\eta\eta} + X_mY_{n,\eta\eta}X_{r,\xi}Y_{s,\eta\eta}) \\
& + \mu^3 D_{26}(X_{m,\xi\xi}Y_nX_{r,\xi}Y_{s,\eta} + X_{m,\xi}Y_{n,\eta}X_{r,\xi\xi}Y_s)\Big]d\xi d\eta \\
L(rs,mn) = & \mu^2\Big[\sum_k c_k\int_{-1}^{1}\int_{-1}^{1}Y_kX_{m,\xi}Y_nX_{r,\xi}Y_sd\xi d\eta + \\
& \sum_{p,q}\phi_{pq}\int_{-1}^{1}\int_{-1}^{1}X_pY_{q,\eta\eta}X_{m,\xi}Y_nX_{r,\xi}Y_sd\xi d\eta + \\
& \sum_{p,q}\phi_{pq}\int_{-1}^{1}\int_{-1}^{1}X_{p,\xi\xi}Y_qX_{m,\xi}Y_nX_{r,\xi}Y_sd\xi d\eta + \\
& \sum_{p,q}\phi_{pq}\int_{-1}^{1}\int_{-1}^{1}X_{p,\xi}Y_{q,\eta}X_{m,\xi}Y_nX_{r,\xi}Y_sd\xi d\eta\Big]
\end{aligned}
\tag{27}
$$

where $m, r = 0, 1, \cdots, M$; $n, s = 0, 1, \cdots, N$ and $rs = (r+1)(N+1)+(s+1)$; $mn = (m+1)(N+1)+(n+1)$.

References

[1] M. Hyer, H. Lee, Use of curvilinear fiber format to improve buckling resistance of composite plates with central circular holes, Composite Structures 18 (3) (1991) 239 – 261.

[2] R. Olmedo, Z. Gürdal, Buckling response of laminates with spatially varying fiber orientations, Collection of Technical Papers - AIAA/ASME Structures, Structural Dynamics and Materials Conference (1993) 2261 – 2269.

[3] S. Nagendra, S. Kodiyalam, J. E. Davis, V. Parthasarathy, Optimization of tow fiber paths for composite design, Collection of Technical Papers - AIAA/ASME/ASCE/AHS/ASC Structures, Structural Dynamics and Materials Conference 2 (1995) 1031 – 1041.

[4] C. Waldhart, Z. Gürdal, C. Ribbens, Analysis of tow placed, parallel fiber, variable stiffness laminates, Collection of Technical Papers - AIAA/ASME/ASCE/AHS/ASC Structures, Structural Dynamics and Materials Conference (1996) 2210 – 2220.

[5] Z. Gürdal, B. Tatting, C. Wu, Variable stiffness composite panels: Effects of stiffness variation on the in-plane and buckling response, Composites Part A: Applied Science and Manufacturing 39 (5) (2008) 911 – 922.

[6] S. T. IJsselmuiden, M. M. Abdalla, Z. Gürdal, Optimization of variable-stiffness panels for maximum buckling load using lamination parameters, AIAA Journal 48 (1) (2010) 134 – 143.

[7] S. Honda, Y. Narita, K. Sasaki, Maximizing the fundamental frequency of laminated composite plates with optimally shaped curvilinear fibers, Journal of System Design and Dynamics 3 (6) (2009) 867–876.

[8] Z. Gürdal, R. Olmedo, In-plane response of laminates with spatially varying fiber orientations. variable stiffness concept, AIAA journal 31 (4) (1993) 751 – 758.

[9] B. F. Tatting, Z. Gürdal, Design and manufacture of elastically tailored tow placed plates, NASA/CR 2002- 211919 (2002) 1–14.

[10] K. C. Wu, Z. Gürdal, Variable stiffness panel structural analyses with material nonlinearity and correlation with tests, Collection of Technical Papers - AIAA/ASME/ASCE/AHS/ASC Structures, Structural Dynamics and Materials Conference 10 (2006) 6772 – 6790.

[11] L. Parnas, S. Oral, U. Ceyhan, Optimum design of composite structures with curved fiber courses, Composites Science and Technology 63 (7) (2003) 1071 – 1082.

[12] S. Setoodeh, A. W. Blom, M. M. Abdalla, Z. Gürdal, Generating curvilinear fiber paths from lamination parameters distribution, Collection of Technical Papers - AIAA/ASME/ASCE/AHS/ASC Structures, Structural Dynamics and Materials Conference 5 (2006) 3440 – 3452.

[13] A. Alhajahmad, M. M. Abdallah, Z. Gürdal, Design tailoring for pressure pillowing using tow-placed steered fibers, Journal of Aircraft 45 (2) (2008) 630 – 640.

[14] S. Setoodeh, M. M. Abdalla, S. T. IJsselmuiden, Z. Gürdal, Design of variable-stiffness composite panels for maximum buckling load, Composite Structures 87 (1) (2009) 109 – 117.

[15] A. F. Martin, A. W. Leissa, Application of the ritz method to plane elasticity problems for composite sheets with variable fibre spacing, International Journal for Numerical Methods in Engineering 28 (8) (1989) 1813–1825.

[16] M. D. Pandey, A. N. Sherbourne, Stability analysis of inhomogeneous, fibrous composite plates, International Journal of Solids and Structures 30 (1) (1993) 37 – 60.

[17] H. Ghiasi, K. Fayazbakhsh, D. Pasini, L. Lessard, Optimum stacking sequence design of composite materials. part ii: Variable stiffness design, Composite Structures 93 (1) (2010) 1 – 13.

[18] E. Lund, L. Khlmeier, J. Stegmann, Buckling optimization of laminated hybrid composite shell structures using discrete material optimization, Proceedings of the 6th World Congress on Structural and Multidisciplinary Optimization (WCSMO6) (2005) 1–10.

[19] J. M. J. F. Van Campen, Z. Gürdal, Retrieving variable stiffness laminates from lamination parameters distribution, 50th AIAA/ASME/ASCE/AHS/ASC Structures, Structural Dynamics and Materials Conference (2009) 1–23.

[20] D. E. Goldberg, Genetic Algorithms in Search, Optimization, and Machine Learning, Addison Wesley Longman, Reading, MA,, 1989.

[21] R. Le Riche, R. T. Haftka, Optimization of laminate stacking sequence for buckling load maximization by generic algorithm, AIAA journal 31 (5) (1993) 951 – 956.

[22] S. Nagendra, R. Haftka, Z. Gürdal, Design of a blade stiffened composite panel by a genetic algorithm, Collection of technical papers -

AIAA/ASME Structures, Structural Dynamics and Materials Conference (pt 4) (1993) 2418 – 2436.

[23] J. Enrique Herencia, P. M. Weaver, M. I. Friswell, Optimization of long anisotropic laminated fiber composite panels with t-shaped stiffeners, AIAA Journal 45 (10) (2007) 2497 – 2509.

[24] K. Washizu, Variational Methods in Elasticity and Plasticity, Second Edition, Pergamon Press, 1975.

[25] E. H. Mansfield, The bending and stretching of plates, Second Edition, Cambridge University Press, 1989.

[26] Y. Tang, X. Wang, Buckling of symmetrically laminated rectangular plates under parabolic edge compressions, International Journal of Mechanical Sciences 53 (2) (2011) 91 – 97.

[27] P. Jana, K. Bhaskar, Stability analysis of simply-supported rectangular plates under non-uniform uniaxial compression using rigorous and approximate plane stress solutions, Thin-Walled Structures 44 (5) (2006) 507 – 516.

[28] Z. Wu, G. Raju, P. M. Weaver, Buckling analysis of vat plate using energy method, Collection of Technical Papers - 53rd AIAA/ASME Structures, Structural Dynamics and Materials Conference (2012) 1–12.

[29] Z. Wu, X. Ma, P. N. Brett, J. Xu, Vibration analysis of submerged rectangular microplates with distributed mass loading, Proceedings of the Royal Society A: Mathematical, Physical and Engineering Sciences 465 (2104) (2009) 1323 – 1336.

[30] R. M. Jones, Mechanics of composite materials, CRC Press, 2nd Revised edition edition, 1998.

[31] Z. Wu, G. Raju, , P. M. Weaver, A comparison of variational, differential quadrature and approximate closed form solution methods for buckling of highly flexurally anisotropic laminates, Journal of Engineering Mechanics(accepted).

[32] E. Braaten, G. Weller, An improved low-discrepancy sequence for multidimensional quasi-monte carlo integration, Journal of Computational Physics 33 (2) (1979) 249 – 258.

[33] E. Kreyszig, Advanced Engineering Mathematics, John Wiley & Sons, 1999.

[34] B. F. Tatting, Analysis and design of variable stiffness composite cylinders, Ph.D. thesis, Virginia Polytechnic Institute and State University (1998).

[35] M. Gupta, S. G. Narasimhan, Legendre polynomials triple product integral and lower-degree approximation of polynomials using chebyshev polynomials (2007) 1–7.

[36] S. Setoodeh, M. M. Abdalla, Z. Gürdal, Design of variablestiffness laminates using lamination parameters, Composites Part B: Engineering 37 (4-5) (2006) 301 – 309.

[37] P. M. Weaver, J. E. Herencia, Buckling of a flexurally anisotropic plate with one edge free, AIAA/ASME/ASCE/AHS/ASC Structures, Structural Dynamics and Materials Conference 8 (2007) 8534 – 8542.

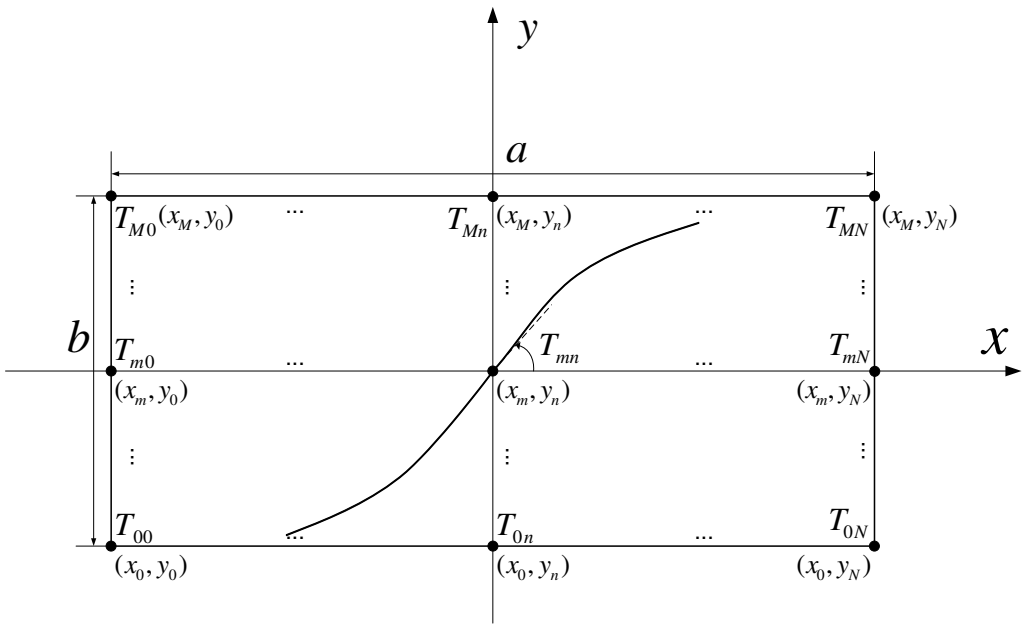

Figure 1: Nonlinear variation of fibre orientation with $M-$ by $-N$ reference points

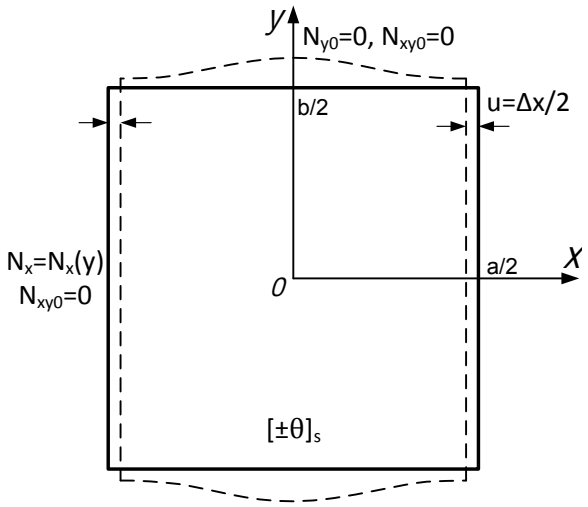

Figure 2: The geometry and in-plane boundary conditions of a VAT plate

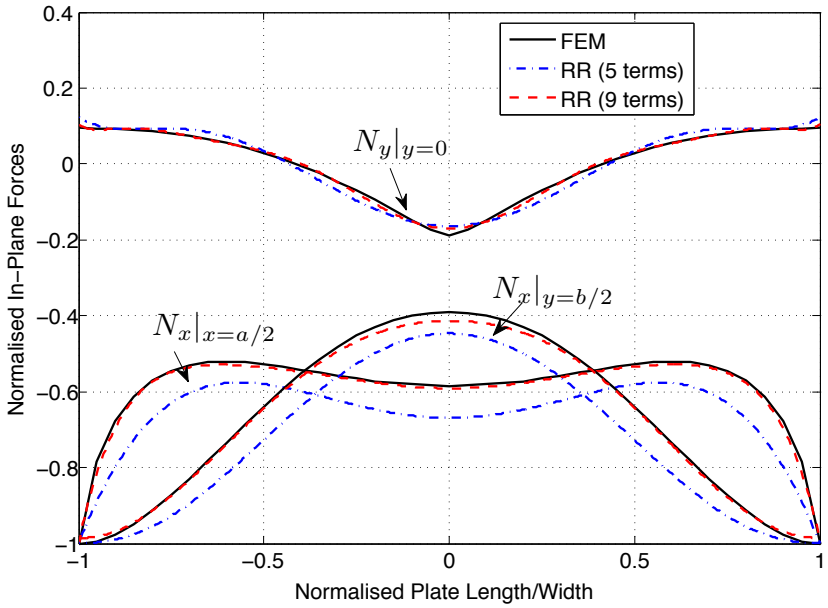

Figure 3: Normalised prebuckling force resultants along different sections for a VAT plate ($[0 \pm \langle 45|0 \rangle]_{2s}$) subjected to uniform displacement compression. Two Rayleigh-Ritz results obtained by using different number of terms in prebuckling force function (Φ) are shown and compared with FEM results.

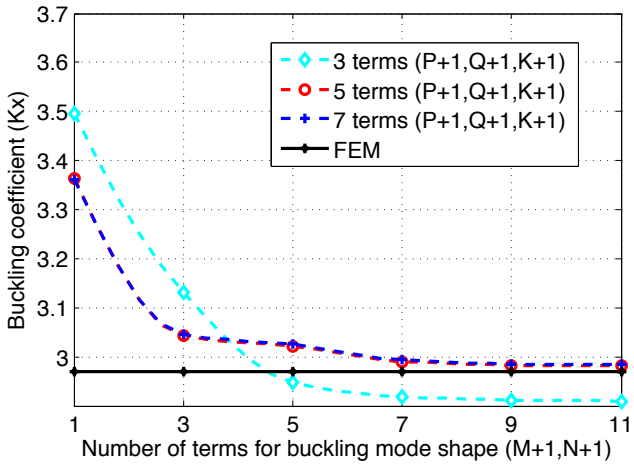

(a)

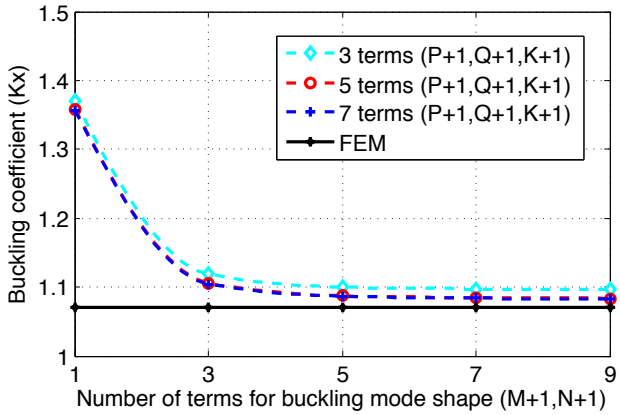

(b)

Figure 4: The convergence trends of applying Rayleigh-Ritz method in the buckling analysis of VAT plates, comparing with FEM results. Different curves represent the prebuckling force distributions are computed by using different number of terms in the force function Φ. Lay-ups: (a) $[90 \pm \langle 0|75\rangle]_{2s}$; (b) $[0 \pm \langle 45|0\rangle]_{2s}$.

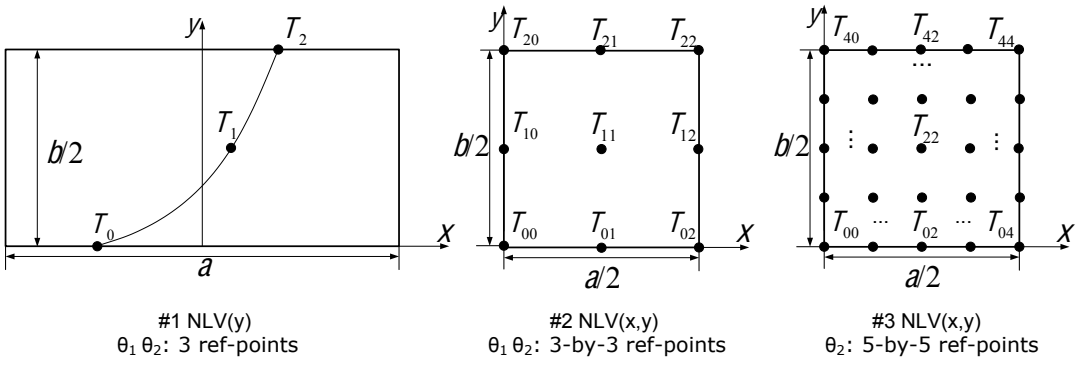

Figure 5: Selection of the reference points in each optimal design

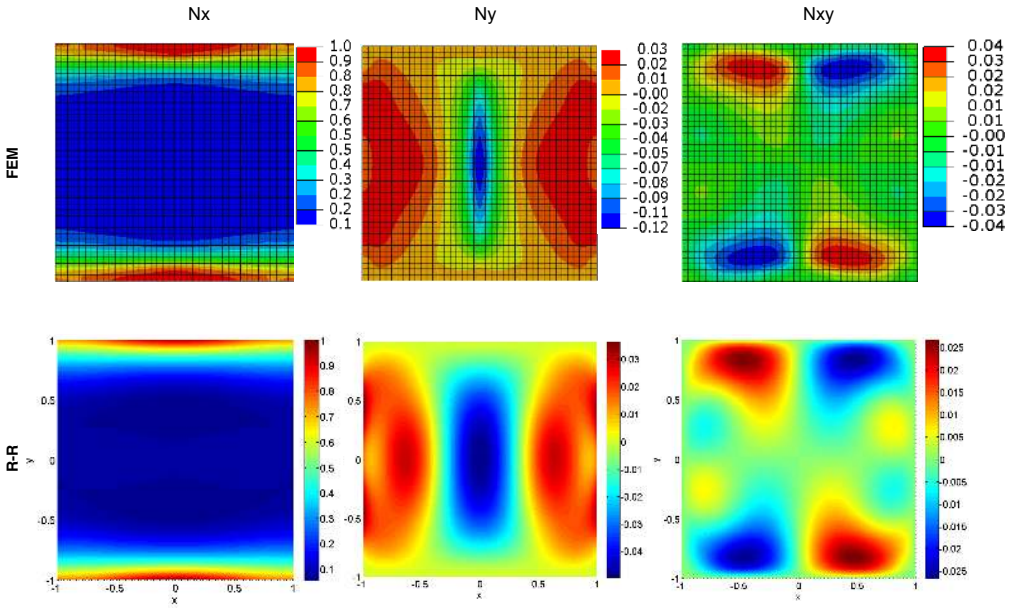

Figure 6: Comparison of FEM and Rayleigh-Ritz results on in-plane stress resultant distribution of the SSSS VAT plate with optimal distribution of fibre angles

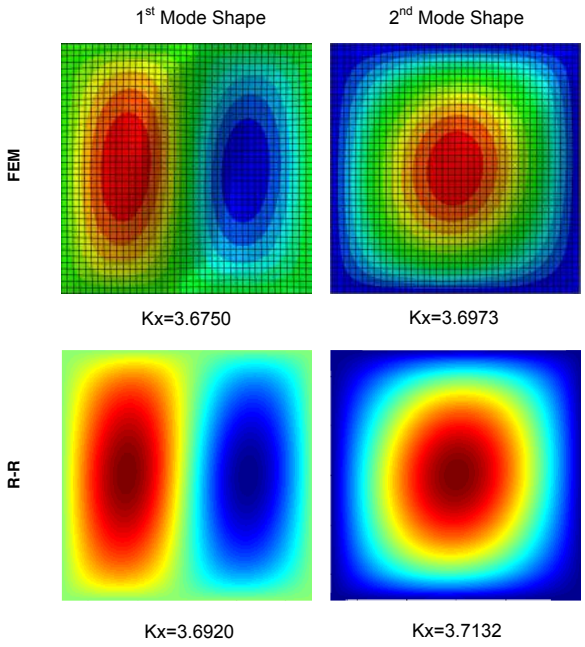

Figure 7: Comparison of FEM and Rayleigh-Ritz results of buckling mode shape of the SSSS VAT plate with optimal distribution of fibre angles

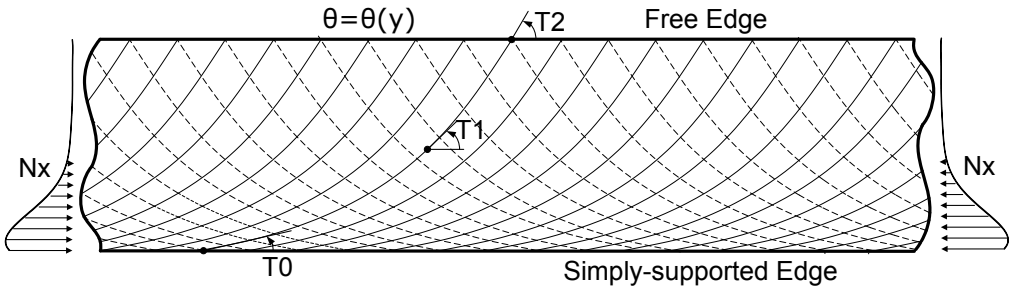

Figure 8: Tow trajectories and load redistribution of SSSF long VAT plate with parabolically varying fibre angles

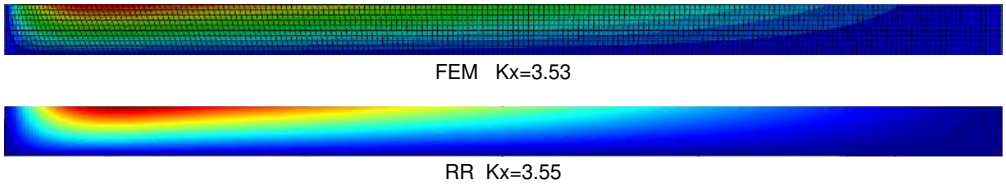

Figure 9: Comparison of FEM and Rayleigh-Ritz results of buckling mode shape and buckling coefficient of the SSSF long VAT plate with optimal distribution of fibre angles